ISSN: 2248-9622, Vol. 15, Issue 11, November 2025, pp 50-62

RESEARCH ARTICLE

OPEN ACCESS

Vanadium-doped nickel cobaltite material for supercapacitor electrodes synthesized via the microwave hydrothermal technique: Augmented structural and electrochemical analysis

BangariBabu Koneti¹, Sathyanarayana Neelam¹, Shilpa Chakra Chidurala², Sadhana Katlakunta¹, Rakesh KumarThida², Md Shareefuddin¹, N.V. Prasad¹, D. Sreenivasu¹, RavinderReddyButreddy¹*

ABSTRACT

Nickel cobaltite is attracting attention as a supercapacitor electrode material as a result of the growing demand for energy storage solutions that are both efficient and effective in regard to the global energy crisis. Introducing transition metals into nickel cobaltite electrodes improves their electrochemical behaviour in energy storage applications. An effective microwave hydrothermal process is used to synthesize a series of $V_x Ni_{1-x}Co_2O_4$ samples where x=0.0 to0.5 with Δx = 0.1. The structural analysis (XRD, FESEM, EDS, FTIR, and XPS) of the samples indicates that they feature a nickel cobaltite cubic spinel structure, which is classified under the Fd-3m space group. The synthesized samples exhibit grain sizes ranging from 80 nm to 127 nm and reveal the presence of multiple oxidation states, notably Ni^{2+}/Ni^{3+} , Co^{2+}/Co^{3+} , and V^{5+} . Electrochemical characterization using cyclic voltammetry (CV), galvanostatic charge—discharge (GCD), and electrochemical impedance spectroscopy (EIS) demonstrated that the $V_{0.3}Ni_{0.7}Co_2O_4$ (VNCO-0.3) electrode achieved a notable specific capacitance, energy density and a power density at a current density of 1 Ag $^{-1}$ in a 2 M KOH electrolyte. So,the VNCO-0.3 electrode sample serves as an effective material for supercapacitor-based energy storage applications.

Keywords: Cubic spinel,nickel cobaltite,microwave hydrothermal, electrochemical, supercapacitor

Date of Submission: 02-11-2025 Date of acceptance: 11-11-2025

I. Introduction

Supercapacitors are widely recognized as complementary energy storage devices owing to their exceptional electrochemical characteristics, such as fast charge-discharge rates, high power density, and extended cycling stability. These attributes render them highly suitable for nextgeneration energy storage technologies. Based on the underlying charge storage mechanisms, supercapacitors are generally categorized into three main types: electric double-layer capacitors (EDLCs), pseudocapacitors (PCs), and hybrid capacitors (HCs) [1-3].In electric double-layer capacitors (EDLCs), energy storage occurs through electrostatic charge accumulation at the electrodeelectrolyte interface, without involving any faradaic (chemical) reactions [4-6]. Conversely, PCs store energy via fast and reversible redox reactions occurring at or near the surface of the electrode in contact with the electrolyte [7–10].

It is important to note that hybrid capacitors (HCs) integrate both electrostatic and

faradaic charge storage mechanisms. Typically, one electrode functions via electric double-layer capacitance, while the other operates through faradaic processes. Both the energy and power density functions of the devices are significantly improved by this synergy. Recently, numerous conducting polymers have been employed to store energy in redox-active transition oxide materials such as MnO₂ and RuO₂ [11-18].

While carbon-based electrodes predominantly confined to electric double-layer capacitors (EDLCs) because of their comparatively low specific and volumetric capacitance [19–21], binary metal oxides with spinel structures (MCo₂O₄, where M denotes transition metals such as Mn, Ni, Zn, Cu, or Mg) have emerged as promising improving alternatives for supercapacitor performance. This is primarily attributed to their fast and reversible redox reactions, excellent structural stability, and superior electrical conductivity [22].

¹Department of Physics, UCS, Osmania University, Hyderabad, Telangana, India

²CentreforNanoScienceandTechnology,JNTU-Hyderabad,Telangana,India

^{*}Corresponding author

Nickel cobaltite (NiCo₂O₄), a spinelstructured material, has gained attention as a potential electrode for supercapacitors due to its cost-effectiveness, environmental compatibility, and abundance of redox-active sites [23, 24]. In parallel, transition metal vanadates such as V₂O₅have garnered significant interest owing to their versatile oxidation states (V5+, V4+, and V3+), which facilitate rich redox activity [25-26]. This characteristic enhances their electrochemical performance and expands their range of potential applications. Various synthesis methods have been employed for the fabrication of nickel cobalt oxide materials, including co-precipitation [27], sol-gel techniques [28], conventional hydrothermal processes [29], and the microwave-assisted hydrothermal approach [30].

Among the diverse synthesis techniques available, the microwave-assisted hydrothermal (MH) method is distinguished by its significant advantages, including homogeneous thermal distribution, enhanced reaction kinetics, and precise control over particle morphology [31–32]. However, there is a scarcity of literature regarding the synthesis of vanadium-doped NiCo₂O₄ using this method. In this study, the MH technique was successfully used to create V-doped NiCo₂O₄ (VNCO) samples. A thorough study was performed to assess the structural and electrochemical effects of vanadium inclusion at the nickel sites within the NiCo₂O₄ lattice.

II. Experimental

Vanadium-substituted NiCo₂O₄ compounds with compositions $V_xNi_{1-x}Co_2O_4$ (x = 0.0 to 0.5) synthesized using accurately measured stoichiometric quantities of nickel nitrate hexahydrate $(Ni(NO_3)_2 \cdot 6H_2O)$, cobalt nitrate hexahydrate $(Co(NO_3)_2 \cdot 6H_2O),$ ammonium metavanadate (NH₄VO₃), and sodium hydroxide (NaOH). These precursors were dissolved in 50 mL of distilled water to form a uniform solution, which was stirred vigorously using a magnetic stirrer to ensure complete mixing. The prepared solution was then transferred into a Teflon-lined stainless steel autoclave and subjected to microwave-assisted hydrothermal treatment at 160 °C for 2 hours in a 1200 W microwave system, with a heating ramp duration of 10 minutes. After the reaction, the autoclave was allowed to cool naturally to ambient temperature, resulting in the formation of a solid precipitate.

Deionized water was used to repeatedly cleanse the precipitates, ensuring complete removal of impurities. The purified samples were subsequently dried in a hot air oven at 80 °C for a

duration of 48 hours to remove residual moisture. The nanopowders were produced by precisely grinding the materials and calcining them at 950°C for 4 hours after drying out. These VNCO nanopowders were subsequently used for various characterization studies, including structural and electrochemical analyses.

Electrochemical evaluations were carried out using a standard three-electrode system comprising a working electrode, a reference electrode, and a counter electrode. To fabricate the working electrode, a homogeneous slurry was prepared by mixing the synthesized VNCO powder, carbon black, and polyvinylidene fluoride (PVDF) in a weight ratio of 80:10:10, with N-methyl-2-pyrrolidone (NMP) serving as the solvent. The resulting slurry was uniformly coated onto a nickel foil current collector and dried at 80 °C for 12 hours. In this configuration, a platinum wire acted as the counter electrode, while an Ag/AgCl electrode was employed as the reference.

The crystal structure and phase purity of the synthesized VNCO materials were examined using X-ray diffraction (XRD) with Cu-Kα radiation. The surface morphology, microstructural features, and elemental distribution were investigated through Field Emission Scanning Electron Microscopy (FESEM) integrated with Energy-Dispersive X-ray Spectroscopy (EDS). Fourier-transform infrared spectroscopy (FTIR) was employed to analyze the vibrational modes of functional groups, while X-ray photoelectron spectroscopy (XPS) was used to determine the oxidation states and chemical environments of the constituent elements.

The electrochemical performance of the VNCO samples was systematically investigated using cyclic voltammetry (CV), galvanostatic charge—discharge (GCD), and electrochemical impedance spectroscopy (EIS). CV measurements were performed within a potential window of –0.1 V to 0.4 V at scan rates of 5, 10, 15, 20, and 25 mV s⁻¹. To assess cycling stability, GCD tests were conducted over 1000 consecutive charge—discharge cycles at a current density of 1 A g⁻¹. EIS analysis was carried out in the frequency range of 0.1 Hz to 10⁵ Hz using 2 M KOH as the electrolyte [33].

III. Interpretations of Results

Figure 1a presents the X-ray diffraction (XRD) patterns of $V_x Ni_{1-x} Co_2 O_4$ samples with varying vanadium concentrations (x = 0.0 to 0.5, in increments of 0.1). The diffraction profiles exhibit sharp and well-resolved peaks, indicative of high crystallinity in the synthesized materials. The observed reflections at 20 values of 18.93°, 31.24°,

36.78°, 38.54°, 44.76°, 55.56°, 59.26°, and 65.08° correspond to the (111), (220), (311), (222), (400), (422), (511), and (440) planes, respectively. These diffraction peaks are consistent with the standard pattern for a face-centered cubic spinel structure of $NiCo_2O_4$, assigned to the *Fd*-3m space group (ICDD card number 01-073-1702).

The crystallite size (D) of the samples was estimated using Scherrer's equation, expressed as:

$$D = \frac{K\lambda}{\beta \cos \theta} \quad nm \qquad ----- (1)$$

Where K denotes the shape factor (commonly taken

as 0.9), λ is the wavelength of the X-ray radiation (0.154 nm), β is the full width at half maximum (FWHM) of the diffraction peak, and θ is the Bragg diffraction angle. The X-ray density (ρ) was determined using the relation:

$$\rho = \frac{ZM}{Na^3} \frac{g}{cm^3} - \dots (2)$$

In this equation, Z represents the number of formula units per unit cell, M is the molar mass of the compound, N is Avogadro's number, and a corresponds to the lattice constant obtained from XRD analysis.

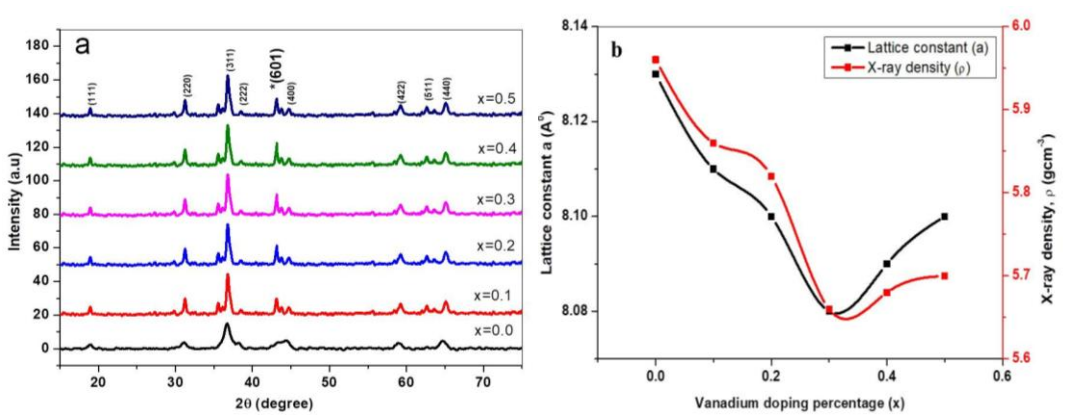


Fig. 1a The XRD patterns and Fig. 1b presents the effect of doping of vanadium on both the lattice parameter and X-ray density of VNCO samples

Figure 1b presents the dependence of the lattice constant (a) and X-ray density (p) on the vanadium doping concentration. The diffraction peak observed at $2\theta = 43.14^{\circ}$, indicated by an asterisk (*), corresponds to the (601) crystallographic plane of VO₂, as identified by the standard reference pattern (JCPDS card No. 31-

1438). According to Scherrer's formula, the size of the crystallites varied between 9.1 A⁰and 14.26 A⁰. The alteration in crystallite size results from micro strain induced in the prepared samples, which affects X-ray density in relation to the vanadium doping percentage.

Table 1 Measured structural parameters of VNCO samples

Sample No.	Vanadium	Lattice Parameter	Average Crystallite Size	X-ray Density
	(x)	<a>(Å)	<d> (nm)</d>	$(\rho) \ (g.cm^{-3})$
1	0.0	8.13	9.10	5.94
2	0.1	8.11	14.15	5.86
3	0.2	8.10	14.26	5.82
4	0.3	8.08	14.12	5.66
5	0.4	8.09	14.15	5.68
6	0.5	8.10	14.17	5.70

The progressive reduction in the lattice parameter (a) with increasing vanadium incorporation is primarily ascribed to the substitution of Ni²⁺ ions by smaller V⁵⁺ ions, resulting in a contraction of the crystal lattice due to the difference in ionic radii. The average crystallite size initially grows with vanadium incorporation but

begins to decline beyond the VNCO (x = 0.3) composition, possibly due to lattice distortion. X-ray density generally decreases with increasing vanadium content, then shows a slight rise after x = 0.3, which can be associated with changes in molar mass and micro strain within the spinel structure.

Figure 2(a-f) presents Field Emission Electron Microscopy (FESEM) micrographs of V_xNi_{1-x}Co₂O₄ samples with varying vanadium content (x = 0.0 to 0.5), providing detailed insights into the surface morphology and elemental distribution as influenced by progressive substitution.All samples vanadium irregularly agglomerated microstructures, with grain sizes ranging from approximately 80 nm to 127 nm. A noticeable change in particle shape occurs as the level of vanadium doping increases.

The undoped $NiCo_2O_4$ (x = 0.0) sample shows a hexagonal morphology, which gradually

transitions to a more spherical form with higher vanadium content. Energy Dispersive X-ray Spectroscopy (EDS) analysis, as shown in Figure 2(g-l), confirms the absence of any extraneous elemental contamination. The detected elements Ni, Co, O, and V are uniformly distributed and exhibit compositional ratios consistent with the theoretical stoichiometry anticipated from the synthesis protocol. The $V_xNi_{1-x}Co_2O_4$ sample with x = 0.3 has smaller particles and a larger surface area, which usually results in improved electrochemical performance, according to similar research on nanoferrites [34].

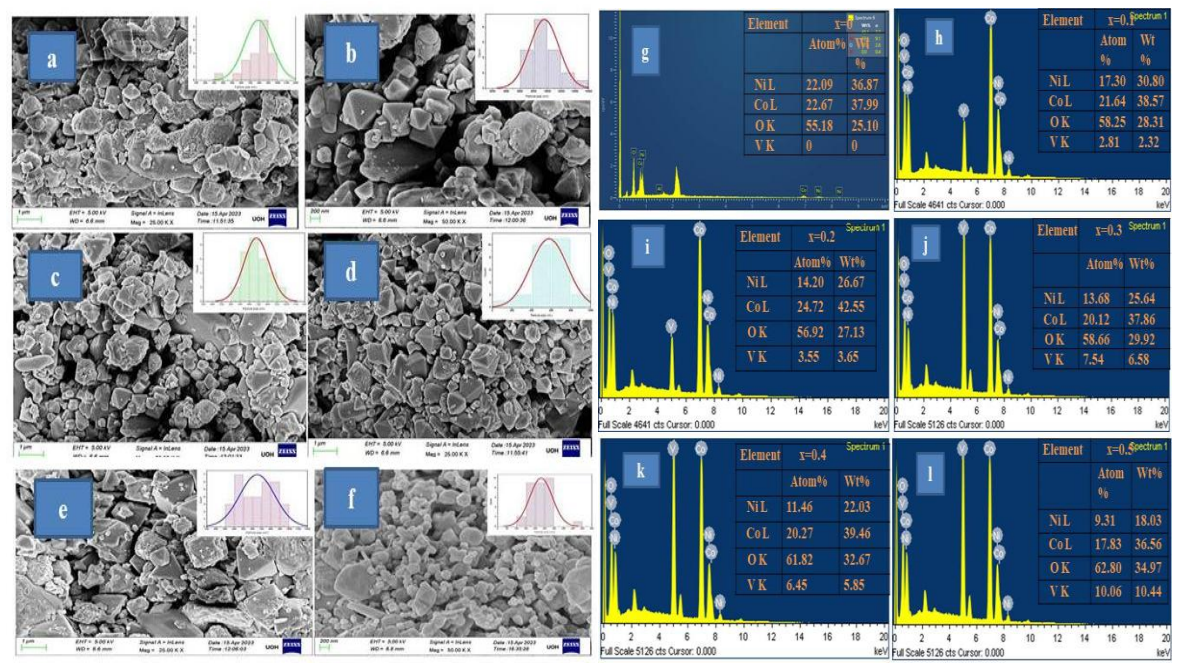


Fig. 2(a-f) FESEM micrographs, and the associated EDS images (Figure 2(g-l)) illustrate the elemental composition, surface features of VNCO materials

The Fourier Transform Infrared (FTIR) spectra (Figure 3) of the VNCO samples reveal distinct absorption bands associated with various functional groups and metal-oxygen bonds. The wide peak seen at 3454.62 cm⁻¹ is due to O-H stretching vibrations, probably caused by moisture that has collected on the sample's surface. The absorption feature around 2362.87 cm⁻¹ corresponds to the asymmetric stretching of CO2 molecules, which may originate from exposure to atmospheric carbon dioxide during the measurement process. The absorption band at 1626.04 cm⁻¹ is associated with H-O-H bending vibrations, indicating the presence of adsorbed moisture within the sample.

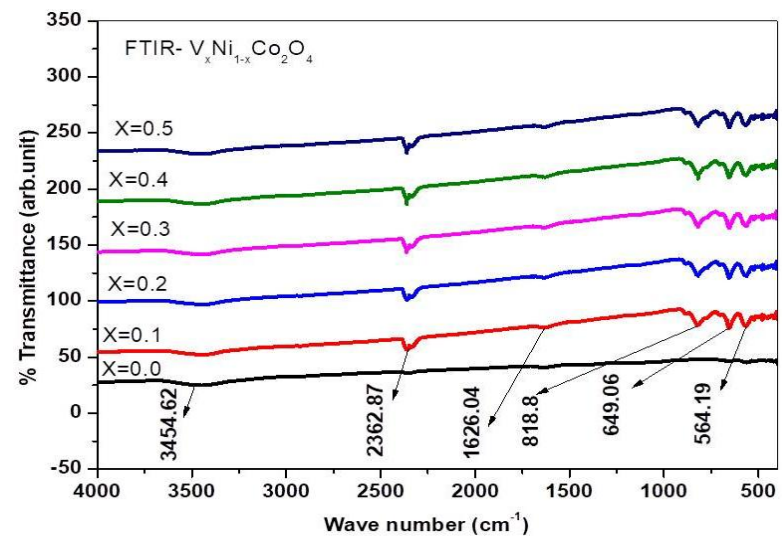


Fig. 3 FTIR spectra of VNCO samples with varying vanadium content (x = 0.0 to 0.5)

Prominent peaks observed at 818.8 cm⁻¹, 649.06 cm⁻¹, and564.19 cm⁻¹correspond tometal—oxygen (M–O) stretching vibrations, which are characteristic of the spinel crystal structure. Notably, a gradual shift of these absorption bands toward higher wavenumbers is observed with increasing vanadium doping concentration [35], suggesting modifications in the local bonding environment. These spectral features are attributed to Ni–O, Co–O, and V–O bonds, confirming the successful incorporation of vanadium into the NiCo₂O₄ lattice without the emergence of secondary phases.

X-ray Photoelectron Spectroscopy (XPS) was employed to examine the chemical composition and oxidation states of the constituent elements in the VNCO samples. Figure 4(a–e) presents the deconvoluted high-resolution XPS spectra for the $V_xNi_{1-x}Co_2O_4$ composition at x=0.3, along with a wide-scan spectrum covering the full elemental range. The analysis confirms the presence of Ni, Co, O, and V, with no detectable signals corresponding to foreign contaminants, indicating high sample purity. Additionally, the optical band gap energies were determined through Gaussian fitting of the absorption edges, and the extracted values are summarized in Table 2.

Table 2Binding energy (in eV) values of Ni, Co, V, and O elements in VNCO samplesat Various Vanadium Concentrations

V Concentration (x)	Ni 2p _{1/2}	Ni 2p _{3/2}	Co 2p,/2	Co 2p _{3/2}	$\begin{array}{c} V \\ 2p_{_{1}\!/_{2}} \end{array}$	$\begin{array}{c} V \\ 2p_{\scriptscriptstyle 3/2} \end{array}$	O 1s
0.0	873.10	855.40	795.40	780.30	_	_	529.60
0.1	875.00	855.60	796.50	781.10	523.98	516.28	530.70
0.2	873.90	855.50	795.00	779.90	524.08	516.58	529.80
0.3	873.00	855.50	795.60	780.20	524.18	516.78	530.00
0.4	874.10	854.60	795.30	780.10	523.08	516.18	529.90
0.5	873.70	854.80	794.80	780.20	523.68	516.28	529.90

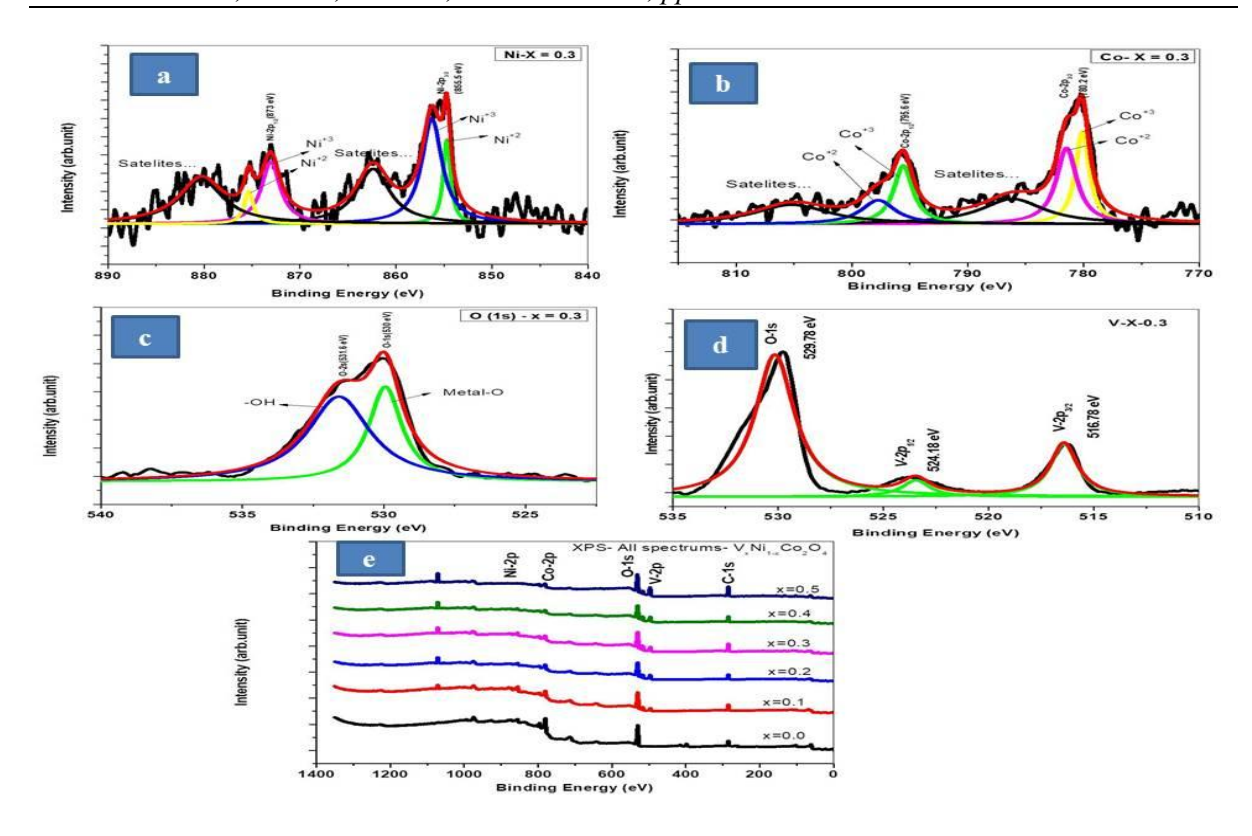


Fig. 4(a-d)deconvoluted XPS spectra of the V_{0.3}Ni_{0.7}Co₂O₄ sample, and Fig. 4(e)the broad XPS spectrum of all VNCO nanopowders

The deconvoluted X-ray Photoelectron Spectroscopy (XPS) spectra reveal that the Ni 2p_{3/2}peaks are located within the range of 854.6 to 855.6 eV, while the corresponding Ni 2p_{1/2} peaks appear between 873.0 and 875.0 eV, accompanied by distinct satellite features. These spectral characteristics indicate the presence of both Ni²⁺ and Ni³⁺ oxidation states within the VNCO samples. Likewise, the Co 2p_{3/2}peaks are observed in the range of 779.9 to 781.1 eV, and the Co $2p_{1/2}$ peaks fall between 794.8 and 796.5 eV, also exhibiting prominent satellite structures. These findings confirm the coexistence of Co²⁺ and Co³⁺species, suggesting mixed-valence states that contribute to enhanced redox activity in the material.

The O 1s XPS spectra, with binding energies observed in the range of 529.6 to 530.7 eV, correspond to metal-oxygen (M-O) bonds within the VNCO lattice, confirming the presence of lattice oxygen. The successful incorporation of vanadium into the spinel framework is evidenced by the presence of V 2p_{1/2} peaks between 523.08 and 524.18 eV, and V $2p_{3/2}$ peaks ranging from 516.18 to 516.78 eV. The observed shifts in binding energy

values with increasing vanadium content imply subtle structural distortions or the development of micro-strain, likely due to the substitution of Ni ions by V ions within the lattice [36]. Moreover, atomic ratios obtained from XPS quantitative analysis, particularly the O/Co/Ni ratio, highlight that compositional modifications at the Ni site play a crucial role in influencing the electrochemical characteristics of the VNCO nanomaterials.

Cyclic voltammetry (CV) measurements were performed for all V_xNi_{1-x}Co₂O₄samples with varying vanadium concentrations (x = 0.0 to 0.5) to evaluate their electrochemical behavior. The corresponding CV curves, recorded over a potential window of -0.1 V to 0.4 Vat scan rates of 5, 10, 15, 20, and 25 mV s⁻¹, are depicted in Figure 5(a-e). As illustrated in Figure 5(f), the calculated specific capacitance exhibits a decreasing trend with increasing scan rate, with the maximum capacitance values obtained at the lowest scan rates. This behavior is attributed to enhanced ion diffusion and greater interaction between the electrolyte and the electrode surface at slower scan rates.

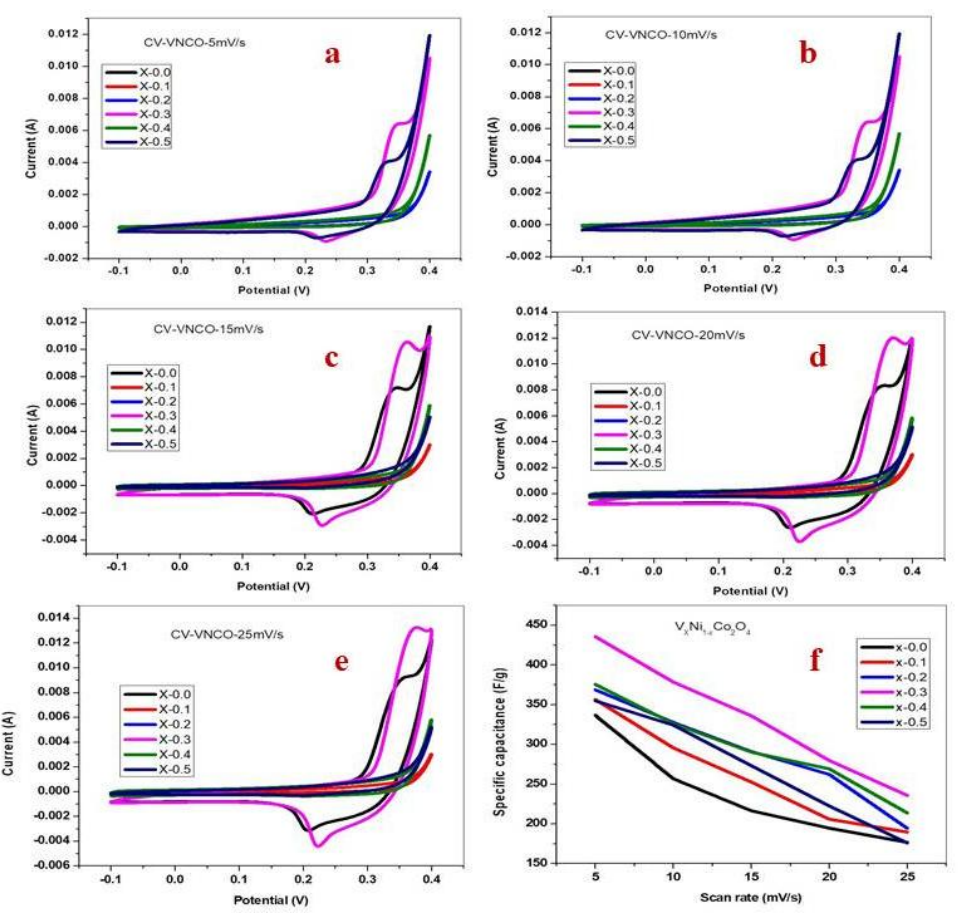


Fig. 5(a-e) cyclic voltammetry profiles of VNCO samples at different scan rates (5, 10, 15, 20, and 25 mV/s), and Fig. 5(f) illustrates the correlation between specific capacitance and scan rate.

The specific capacitance (C_s) of the samples was calculated from the cyclic voltammetry (CV) data using the following relation:

$$C_s = \frac{\int I dv}{2 m * V s * \Delta V} F g^{-1} - \cdots (3)$$

 ${\it C}_s = \frac{\int I dv}{2 \; m*Vs*\Delta V} F \; g^{-1} ----- (3)$ where I(V) is the current as a function of voltage, m is the mass of the active material deposited on the electrode (in grams), v is the scan rate (in V s⁻¹), and ΔV represents the potential window used during the measurement.

The CV curves depicted in Figure 5(a-e) show asymmetrical oxidation and reduction peaks, indicating a kinetically irreversible redox behavior of the ions. As presented in Table 3, the specific capacitance increases with higher vanadium content but decreases with rising scan rates, reaching its maximum at lower scan rates. The specific capacitance typically increases when doping enhances redox activity and electrical conductivity.

Table 3Calculated specific capacitance (Cs) values of all VNCO samples at different potential scan rates

S.No	Potential scan rates (mVs ⁻¹)	specific capacitance values (C _s) of V _x Ni _{1-x} Co ₂ O ₄ samples with x=0.0 to 0.5 (Fg ⁻¹)							
		0.0	0.1	0.2	0.3	0.4	0.5		
1	5	336.5	356.3	368.7	435.5	375.3	354.8		
2	10	256.5	295.4	327.6	378.2	326	324		
3	15	216.2	252.4	290.8	335.7	290	273		
4	20	194.3	205.7	262	279.6	269	222.3		
5	25	176.4	189.5	194.2	235.6	213.5	175.7		

In vanadium-doped $NiCo_2O_4$, the incorporation of V^{5+} ions with variable oxidation states facilitates enhanced redox activity and reduces charge transfer resistance, thereby improving the specific capacitance. Nevertheless, an excessive amount of vanadium can introduce structural defects, disturb the redox-active framework, or lead to particle agglomeration, all of which can negatively impact the electrochemical performance.

Within the $V_x Ni_{1-x} Co_2 O_4$ series, the composition with x=0.3 exhibited superior specific capacitance and improved electrochemical reversibility, especially at reduced scan rates. This improvement is primarily ascribed to the prolonged duration available for effective ion diffusion and charge transfer within the electrode matrix under lower scanning rates. The prominent loop area observed for x=0.3 suggests a greater density of redox-active sites, with a redox peak current reaching approximately 7 mA. This behavior may

result from its higher crystallinity, reduced lattice parameter (a = 8.10 A^0), and increased surface area.

Figure 5(f) illustrates that specific capacitance generally decreases with increasing scan rate, yet shows an upward trend with higher vanadium content. These findings indicate that the x=0.3 sample possesses efficient charge storage characteristics and superior capacitance performance. Moreover, the incorporation of vanadium ions appears to enhance ionic transport within the porous framework of the NiCo₂O₄ structure [37–41].

Figure 6 presents the galvanostatic charge—discharge (GCD) profiles of $V_x Ni_{1-x} Co_2 O_4 samples$ with varying vanadium content (x=0.0 to 0.5, with $\Delta x=0.1$), recorded at a constant current density of 1 A g^{-1} within a potential window of–0.1 V to 0.4 V, using 2 M KOH as the electrolyte. Among all the compositions investigated, the sample with x=0.3 demonstrated the longest discharge time, reaching approximately 400 seconds, indicating superior charge storage capacity under the given conditions.

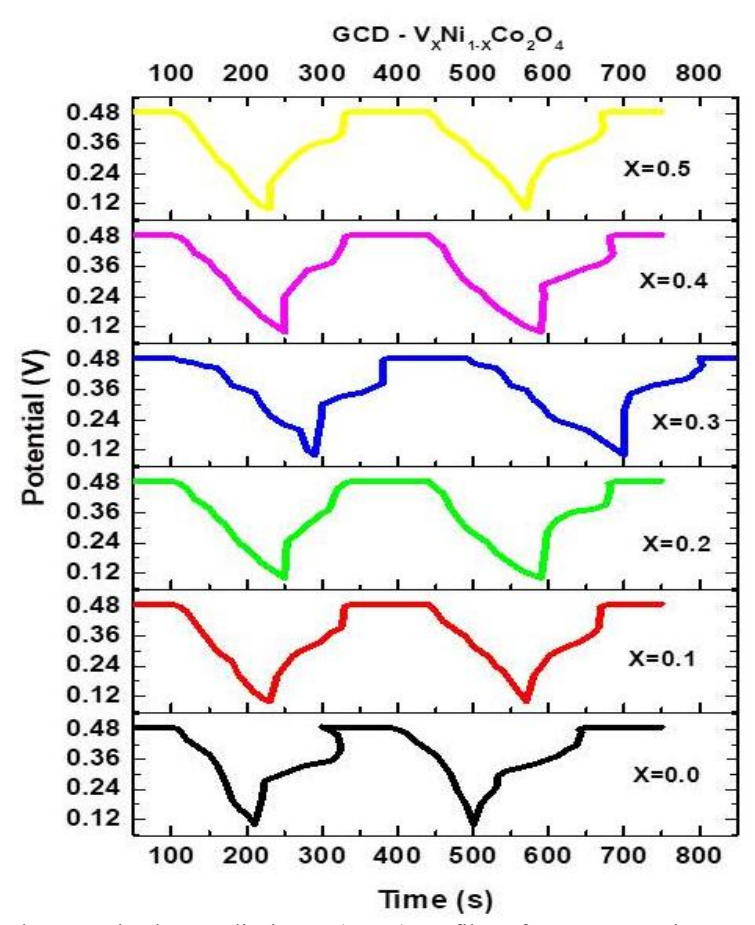


Fig. 6 Illustrates galvanostatic charge-discharge (GCD) profiles of VNCO samples at current density 1 Ag⁻¹

The specific capacitance (C_s), energy density (E_d), and power density (P_d) of the $V_xNi_{1-x}Co_2O_4$ samples

were quantitatively evaluated using established electrochemical equations derived from

galvanostatic charge–discharge (GCD) measurements, as follows:

$$C_{s} = \frac{Ix \, \Delta t}{\text{mx } \Delta V} \text{Fg}^{-1} \quad ----- (4)$$

$$E_{d} = \frac{C_{s} \, (\Delta V)^{2}}{2} (\frac{10}{36}) \quad \text{Whkg}^{-1} \quad ----- (5)$$

$$P_{d} = (\frac{E_{d}}{\Delta t}) x 3600 \text{Wkg}^{-1} ----- (6)$$

where C_s (F g^{-1}) denotes the specific capacitance, I (A) is the applied constant current, Δt (s) is the discharge time, m (g) represents the mass of the

active electrode material, and $\Delta V \; (V)$ is the applied potential window.

Table 4 presents a comprehensive summary of the calculated values of specific capacitance (C_s), energy density (E_d), and power density (P_d) for the $V_x Ni_{1-x} Co_2 O_4 samples$, as determined from the galvanostatic charge—discharge (GCD) measurements. Figure 7 depicts how these electrochemical parameters vary with different vanadium doping levels in the synthesized VNCO samples.

Table 4 Measured electrochemical characteristics of VNCO samples

S.NO	Parameters	Concentration of V in VNCO samples (x = 0.0 to 0.5)						
		0.0	0.1	0.2	0.3	0.4	0.5	
1	Specific capacitance (C _s) Fg ⁻¹	242.1	285.6	330.3	412.5	320	275.7	
2	Energy density (E _d) Whkg ⁻¹	6.21	7.67	9.28	12.12	9.0	7.754	
3	Power density (P _d) Wkg ⁻¹	214.9	219.9	224.8	243.05	210.9	225.0	

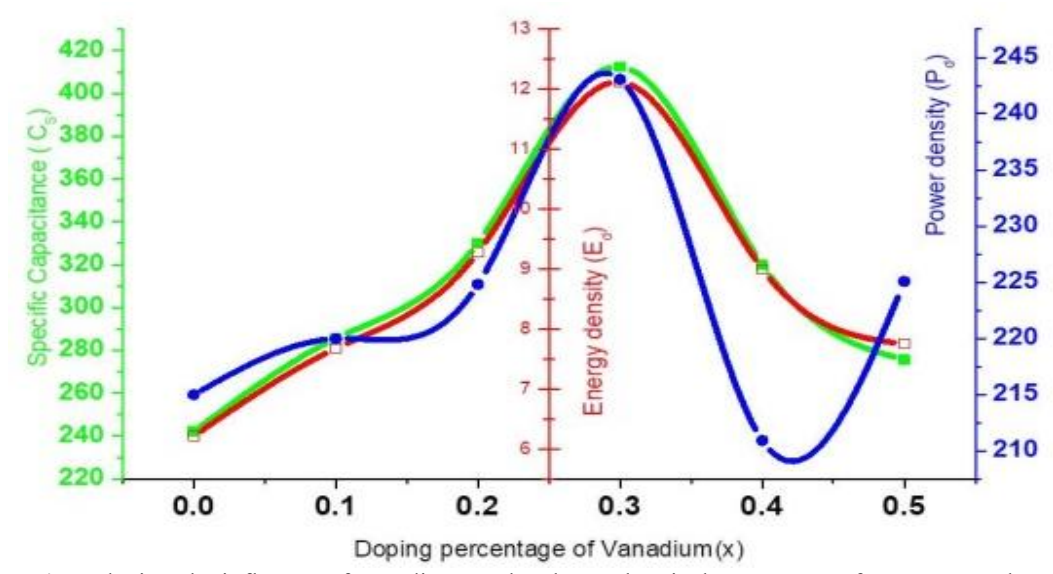


Fig. 7 depicts the influence of vanadium on the electrochemical parameters of VNCO samples

The incorporation of vanadium into the $NiCo_2O_4$ lattice notably enhances the electrochemical interaction between the electrode material and the electrolyte, leading to improved charge—discharge performance, structural stability, and specific capacitance. Among the synthesized compositions, the $V_{0.3}Ni_{0.7}Co_2O_4$ sample exhibits the most favorable electrochemical characteristics, delivering a specific capacitance of 412.5 F g^{-1} , anenergy density of 12.12 Wh kg^{-1} , and apower

density of 243.05 W kg⁻¹ at a current density of 1Ag⁻¹. This enhanced performance is primarily attributed to the improved electrical conductivity and optimized redox activity resulting from vanadium incorporation [42–46].

Electrochemical Impedance Spectroscopy (EIS) was employed to investigate the capacitive behavior, charge transfer dynamics, and electrical conductivity of the electrode materials. The

resulting Nyquist plot, shown in Figure 8(a), depicts the relationship between the real (Z') and imaginary (Z'') components of impedance across a frequency range of 0.1 Hz to 10^5 Hz. The impedance profile of the supercapacitor electrodes reflects contributions from both resistive and capacitive elements. At high frequencies, the system demonstrates a predominantly capacitive response, as evidenced by

the semicircular arc on the right side of the plot, which is typically associated with charge transfer resistance at the electrode–electrolyte interface. Conversely, the low-frequency region, represented by the leftward portion of the plot, is indicative of diffusion-controlled processes and reveals more resistive behavior, related to ion transport within the porous electrode structure.

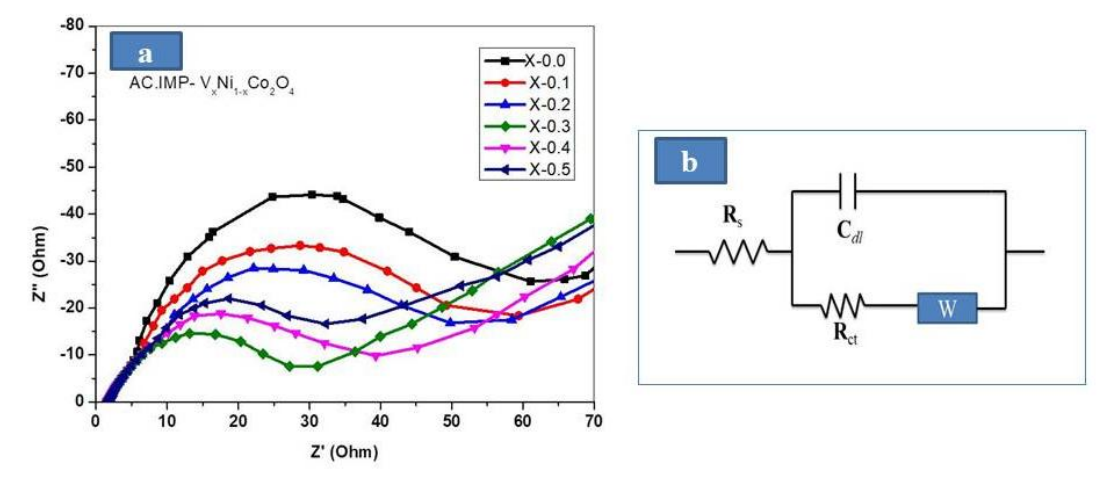


Fig. 8a shows Nyquist plots of $V_xNi_{1-x}Co_2O_4$ samples with varying vanadium content (x = 0.0 to 0.5), and 8b represents the corresponding electrical equivalent circuit model

Interfacial interactions between the electrode surface and the electrolyte are indicated by the significant increase in the high-frequency region of the Nyquist plot. This response is characteristic of the material's blocking capacitance. The angle made by the tangent drawn to the spike of the semi-circle at x=0.3 composition found to be higher than other compositions indicating higher value of capacitance. It also has semi-circle with least radius indicating a minimum bulk resistance. Therefore we can conclude that the vanadium composition at x=0.3 exhibits maximum specific capacitance value which is also confirmed by the cyclic voltammetry studies and also the GCD test.

A reduced semicircle diameter in the Nyquist plot signifies a lower charge-transfer resistance (R_{ct}), which is typically associated with improved charge storage capability and enhanced specific capacitance of the electrode material [47]. The equivalent circuit model used to interpret the impedance data, shown in Figure 8(b), includes R_s(electrolyte resistance), C_{dl} (double-layer capacitance), and R_{ct} (charge-transfer resistance). Among the tested compositions, the V_{0.3}Ni_{0.7}Co₂O₄ electrode demonstrated the most favorable electrochemical performance, exhibiting higher specific capacitance, energy density, and power These enhancements are primarily attributed to its reduced Rct and superior electrical

conductivity.

IV. Conclusions

Vanadium-doped nickel cobaltite (VNCO) electrode materials were synthesized using a microwave-assisted hydrothermal method, followed by a calcination process. Structural analysis confirmed the formation of a well-defined cubic spinel NiCo₂O₄ phase, crystallizing in the Fd-3m space group. Among the various compositions, the VNCO-0.3 sample exhibited the smallest particle dimensions and the largest surface area. X-ray photoelectron spectroscopy (XPS) identified multiple valence states, including Ni2+/Ni3+, Co²⁺/Co³⁺, and V⁴⁺/V⁵⁺, indicating rich redox activity. Electrochemical analysis demonstrated that the VNCO-0.3 electrode delivered a specific capacitance of $412 \, F \, g^{-1}$, with an associated energy density of $12 \, Wh \, kg^{-1}$ and a power density of 243 W kg⁻¹ at a current density of 1 A g⁻¹. These results emphasize the considerable promise of VNCO-0.3 as a high-performance electrode material for supercapacitor applications, attributed to its enhanced charge storage efficiency.

Acknowledgement

The authors express their sincere gratitude to the Head of the Department of Physics and the Dean, Faculty of Science, Osmania University, for their unwavering support and encouragement throughout the course of this research.

Contributions from authors

All authors made significant contributions to the research. BB was responsible for material synthesis and data collection; RK performed the cyclic voltammetry measurements; SK provided critical manuscript revisions; ChSC developed the experimental methodology; BRR and BL carried out the data analysis; and BRR authored the paper.

Research Funding

No external financial support or grants were received for the execution of this research.

Research Data Access

The corresponding author may share the datasets used in this work upon receipt of a valid request.

Declaration of Interests

No conflicts of interest are associated with this publication.

References

- [1]. C. Meng, C. Liu, L. Chen, C. Hu, S. Fan, Highly Flexible and All-Solid-State Paper like Polymer Supercapacitors, Nano Letters. 10 (2010) 4025-4031.
- [2]. S. Park, S. Jayaraman, Smart Textiles: Wearable Electronic Systems, MRS Bulletin. 28 (2011) 585-591.
- [3]. H.D. Abruña, Y. Kiya, J.C. Henderson, Batteries and electrochemical capacitors, Physics Today. 61 (2008) 43-47.
- [4]. Y.J. Lee, H.W. Park, U.G. Hong, I.K. Song, Mn-doped activated carbon aerogel as electrode material for pseudo-capacitive supercapacitor: Effect of activation agent, Current Applied Physics. 12 (2012) 1074-1080.
- [5]. J. Chen, J. Xu, S. Zhou, N. Zhao, C.-P. Wong, Nitrogen-doped hierarchically porous carbon foam: A free-standing electrode and mechanical support for high-performance supercapacitors, Nano Energy. 25 (2016) 193-202.
- [6]. W. Yang, M. Ni, X. Ren, Y. Tian, N. Li, Y. Su, X. Zhang, Graphene in Supercapacitor Applications, Current Opinion in Colloid & Interface Science. 20 (2015) 416-428.
- [7]. Z. Peng, X. Liu, H. Meng, Z. Li, B. Li, Z. Liu, S. Liu, Design and tailoring of the 3D

- macroporous hydrous RuO₂ hierarchical architectures with a hard-template method for high-performance supercapacitors, ACS Applied Materials & Interfaces. 9 (2017) 4577-86.
- [8]. K.R. Prasad, N. Miura, Electrochemically synthesized MnO2-based mixed oxides for high performance redox supercapacitors, Electrochemistry Communications. 6 (2004) 1004-08.
- [9]. Y. Jiang, J. Liu, Definitions of pseudocapacitive materials: a brief review, Energy & Environmental Materials. 2 (2019) 30-37.
- [10]. H. Liu, X. Liu, S. Wang, H.-K. Liu, L.J.E.S.M. Li, Transition Metal based Battery-Type Electrodes in Hybrid Supercapacitors: A Review. 28 (2020) 122-145.
- [11]. Zhi M, Xiang C, Li J, Li M, Wu N, Nanostructured carbonmetal oxide composite electrodes for supercapacitors: a review, Nanoscale. 5 (2013) 72–88.
- [12]. Anwar AW, Majeed A, Iqbal N, Ullah W, Shuaib A, Ilyas U, Rafque HM (2015) Specific capacitance and cyclic stability of graphenebased metal/metal oxide nanocomposites: a review, J Mater Sci. Technol. 31 (2015) 699–707.
- [13]. Cottineau T, Toupin M, Delahaye T, Brousse T, Bélanger D, Nanostructured transition metal oxides for aqueous hybrid electrochemical supercapacitors, Appl Phys A. 82 (2006) 599–606.
- [14]. Snook GA, Kao P, Best AS Conducting-polymer-based supercapacitor devices and electrodes, J Power Sour. 196 (2011) 1–12.
- [15]. Wang H, Lin J, Shen ZX, Polyaniline (PANI) based electrode materials for energy storage and conversion, J SciAdv Mater Devices. 1 (2016) 225–255.
- [16]. Deng W, Ji X, Chen Q, Banks CE, Electrochemical capacitors utilizing transition metal oxides: an update of recent developments, RSC Adv. 1 (2011) 1171–1178.
- [17]. Mastragostino M, Arbizzani C, Soavi F, Conducting polymers as electrode materials in supercapacitors, Solid State Ion. 148 (2002) 493–498.
- [18]. Moussa M, El-Kady MF, Zhao Z, Majewski P, Ma J, Recent progress and performance evaluation for polyaniline/graphene nanocomposites as supercapacitor electrodes, Nanotechnology. 27 (2016) 442001.
- [19]. M. Yanilmaz, M. Dirican, A.M. Asiri, X. Zhang Flexible polyaniline-

- carbonnanofibresupercapacitorelectrodesJour nal of EnergyStorage, 24(2019)100766.
- [20]. S. Ma, Y. Wang, Z. Liu, M. Huang, H. Yang, Z. Xu Preparation of carbon nanofibre withmultilevel gradient porous structure for supercapacitor and CO₂ adsorption Chem. Eng.Sci.,205 (2019)181-189.
- [21]. Y. Luan, G. Nie, X. Zhao, N. Qiao, X. Liu, H. Wang, X. Zhang, Y. Chen, Y.-Z. Long theintegrationofSnO₂dotsandporouscarbonna nofibresforflexiblesupercapacitorsElectrochi mActa,308 (2019)121-130.
- [22]. Liu S, Ni D, Li H-F, Hui KN, Ouyang C-Y, Jun SC, Effect of cation substitution on the pseudo capacitive performance of spinel cobaltite MCo_2O_4 (M = Mn, Ni, Cu and Co), J Mater Chem A. 6 (2018) 10674-10685.
- [23]. Salunkhe RR, Jang K, Yu H, Yu S, Ganesh T, Han S-H, Ahn H, Chemical synthesis and electrochemical analysis of nickel cobaltite nanostructures for supercapacitor applications, J AlloyCompd. 509 (2011) 6677-6682.
- [24]. Dubal D.P, Gomez-Romero P, Sankapal BR, Holze R, Nickel cobaltite as an emerging material for supercapacitors: An overview, Nano Energy. 11 (2015) 377–399.
- [25]. Fang, D. et al. Self-assembled hairy ball-like V₂O₅ nanostructures for lithium ion batteries. RSC Adv. 4(2014) 25205-25209.
- [26]. Afyon, S. et al. New High Capacity Cathode Materials for Rechargeable Li-ion Batteries: Vanadate-Borate Glasses. Scientific Reports 4(2014) 7113.
- [27]. L. Hu, L. Wu, M. Liao, X. Hu, X. Fang, Electrical Transport Properties of Large, Individual NiCo₂O₄ Nanoplates, Adv. Funct. Mater. 22 (2012) 998-1004. https://doi.org/10.1002/adfm.201102155.
- Wonga, J. Wanga, G.BeeTehb, [28]. Y.C. Structural and magnetic studies of SrFe₁₂O₁₉ by sol-gel method, Proc. Eng. 76 (2014) 45
 - http://dx.doi.org/10.1016/j.proeng.2013.09.24
- [29]. S. Vijayakumar, S. Nagamuthu, Muralidharan, Supercapacitor Studies on NiONanoflakes Synthesized Through a Microwave Route, ACS Appl. Mater. 2188-2196. Interfaces. 5 (2013)https://doi.org/10.1021/am400012h.
- [30]. SadhanaKatlakunta, M. Srinivas, Sher Singh Meena, S. Srinath, M. Bououdina, R. Sandhya and K. Praveena, Improved magnetic properties of Cr³⁺ doped SrFe₁₂O₁₉ synthesized via microwave hydrothermal route, Mater. Res. Bull. 63 (2015) 58-66.

www.ijera.com

- https://doi.org/10.1016/j.materresbull.2014.1
- [31]. S. Komarneni., Nanophase materials by hydrothermal, microwave- hydrothermal and microwave-solvothermal methods, Curr. Sci. 85 (2003) 1730-1734.
- [32]. Meng, L.-Y, Wang, B, Ma, M.-G, & Lin, K.L., The progress of microwave-assisted hydrothermal method in the synthesis of functional nanomaterials, Materials Today Chemistry. 1-2 (2016)63-83. Doi:10.1016/j.mtchem.2016.11.003.
- [33]. Sathyanarayana, M., Sriramulu, G., Shilpa Chakra, Ch., Sadhana, K., Venkata Narayana, M., Srinivasu, D., Ravinder Reddy, B., Enhanced structural and Electrochemical properties of Zn-doped NiCo₂O₄ synthesized by Low temperature Microwave Hydrothermal Process, ECS Journal of Solid State Science and Technology. 12 (2023) 093008. DOI: 10.1149/2162-8777/acf4bc.
- [34]. JiaxinHao, Wenjie Wu, Qiao Wang, De Yan, GuohanLiuc and Shanglong Peng, Effect of grain size on electrochemical performance and kinetics of Co3O4 electrode material, RSC J. Mater. Chem. A. (2020) 1-5. DOI: 10.1039/D0TA02032J.
- HaeWoong Park, Byung-Ki Na, Byung Won Cho, Sun-Min Park and Kwang ChulRoh., Influence of vanadium doping on the electrochemical performance of nickel oxide in supercapacitors, RSC (PCCP) Phys. Chem. Chem. Phys. 15 (2013) 17626-17635. DOI: 10.1039/c3cp52498a.
- J.F. Marco, J.R. Gancedo, M. Gracia, J.L. [36]. Gautier, E. Ríos, F.J. Berry, Characterization of the Nickel Cobaltite, NiCo2O4, Prepared by Several Methods: An XRD, XANES, EXAFS, and XPS Study, Journal of Solid State Chemistry. 153 (2000) 74-81.
- PrashanthJampaniHanumantha, Kanchan Datta, Karan Sandeep Kadakia, Dae Ho Hong, Sung Jae Chung, Michael C. Tam, James A. Poston, AyyakkannuManivannan and Prashant N. Kumta, A Simple Low Temperature Synthesis of Nanostructured Vanadium Nitride for Supercapacitor Applications, Journal of The Electrochemical Society. 160 (11) (2013) A2195-A2206. DOI: 10.1149/2.081311jes.
- [38]. Zein K. Heiba, Mohamed Bakr Mohamed, Adel Maher Wahba, M. I. Almalowi, Effect of vanadium doping on structural and magnetic properties of defective nano-nickel ferrite, Applied Physics A Material science and Processing. 124 (2018) 290. https://doi.org/10.1007/s00339-018-1721-3

61 | Page

- [39]. D. Govindarajan, V. Uma Shankar, R. Gopalakrishnan, Supercapacitor behavior and characterization of RGO anchored V₂O₅nanorods, Journal of Materials Science: Materials in Electronics. Springer. (2019). https://doi.org/10.1007/s10854-019-019849
- [40]. Shin J et al, Carbon-coated V₂O₅ nanoparticles with enhanced electrochemical performance as a cathode material for lithium ion batteries, J Alloy Compd. 589 (2014) 322-329.
- [41]. Mondal, S. Maiti, S. Mahanty, A. Baran Panda, Large-scale synthesis of porous NiCo₂O₄ and rGO-NiCo₂O₄ hollow-spheres with superior electrochemical performance as a faradaic electrode, Journal of Materials Chemistry A. 5 (2017) 16854-16864.
- [42]. H. Wei, J. Zhu, S. Wu, S. Wei, Z. Guo, Electrochromic polyaniline/graphite oxide nanocomposites with electrochemical energy storage, Polymer. 54 (2013) 1820-31.
- [43]. K. Tao, Y. Yang, C. Yang, Q. Ma, L. Han, Construction of NiCo2O4nanosheet-decorated leaflike Co₃O₄nanoarrays from metal-organic framework for high-performance hybrid supercapacitors, Dalton Transactions. 48 (2019) 14156-14163.
- [44]. Z. Wang, X. Hu, L. Wang, B. Jin, G. Zou, Z. Huang, Q. Liu, G. Hu, K. Zhang, J.H. Park, Rationally designed hybrids of NiCo₂O₄ and polymeric carbon nitride as faradaic electrodes with enhanced electrochemical performance, ElectrochimicaActa. 299 (2019) 717-726.
- [45]. Q. Zhou, X. Wang, Y. Liu, Y. He, Y. Gao, J. Liu, High rate capabilities of NiCo₂O₄-based hierarchical superstructures for rechargeable charge storage, J. of the electrochemical society. 161 (2014) A1922-A1926.
- L. Gao, J.U. Surjadi, K. Cao, H. Zhang, P. Li, S. Xu, C. Jiang, J. Song, D. Sun, Y. Lu, Flexible fiber-shaped supercapacitor based on nickel-cobalt double hydroxide and pen ink electrodes on metallized carbon fiber, ACS applied materials&interfaces. 9 (2017) 5409-
- [47]. B.-A. Mei, O. Munteshari, J. Lau, B. Dunn, L. Pilon, Physical interpretations of Nyquist plots for EDLC electrodes and devices, The Journal of Physical Chemistry C. 122 (2017) 194-206